Mechanics of Materials 4 (1985) 395–407
North-Holland

INFLUENCE OF YIELD SURFACE CURVATURE ON FLOW LOCALIZATION IN DILATANT PLASTICITY

M.E. MEAR and J.W. HUTCHINSON

Division of Applied Sciences, Harvard University, Cambridge, MA 02138, U.S.A.

Received 8 March 1985; revised version received 7 October 1985

In this paper a family of dilatant plasticity theories is introduced by considering yield surfaces which change according to a combination of isotropic expansion and kinematic translation. One limiting member of the family is Gurson's (1977) isotropic hardening model, and the other limiting member is a pure kinematic hardening version. The family of constitutive laws is constructed such that all versions coincide for proportional stressing histories. The differences between any two versions show up only under nonproportional stressing histories, such as those encountered in many plastic instability phenomena. Under nonproportional stressing, the kinematic version is significantly 'less stiff' than Gurson's isotropic hardening model due to the relatively higher curvature of the kinematic yield surface. This effect is explored in some basic shear localization calculations and is found to have substantial influence on the localization predictions.

1. Introduction

Small volume concentrations of voids can substantially alter the plastic deformation behavior of metals rendering the material highly susceptible to flow localization in the form of shear bands or separation bands. Such localizations tend to lead to material failure, and thus their onset usually marks the termination of permissible straining. Observations of metals that have failed by the ductile void growth mechanism reveal that void volume concentrations outside the localization can be very low, often well below one percent. The implication is that the localization process sets in at correspondingly low void volume fractions. Some high strength metal alloys display little evidence of any voids outside the localization band suggesting that localization may be triggered by nucleation of the voids or, possibly, by a synergistic combination of nucleation and low hardening.

Theories of dilatational plasticity incorporate the contribution to inelastic straining from the nucleation and growth of voids. While such theories will invariably be phenomenological in character, it is essential that they accurately reflect, or model, actual void nucleation and growth processes. A prototype theory has been proposed by Gurson (1977) and, to date, this theory appears to have been applied more than any other. Gurson's theory is endowed with a yield condition, a flow law, a measure of void volume fraction, a rule for nucleating voids, and a law for the evolution of the void volume fraction. Its yield surface was derived from approximate solutions to problems for a volume element of perfectly-plastic material containing a void (a thick spherical shell), and it was extended to strain hardening materials under the assumption of isotropic hardening. The stress–strain behavior of the void-free material is part of the specification of the theory, and with no voids present the Gurson model reduces to the classical Prandtl–Reuss isotropic hardening theory based on the Mises invariant (i.e., J_2 flow theory).

It is well known that the classical J_2 flow theory tends to be 'overly stiff' when used to predict plastic instabilities such as buckling and necking when those instabilities involve distinctly nonproportional stress histories. The low curvature of the isotropic hardening yield surface results in less strain change for a given finite, nonproportional stress change than would be the case for a yield surface with either higher curvature

or a corner at the loading point. Such differences can be substantial for materials with appreciable strain hardening. In a study of sheet metal necking, Tvergaard (1978) invoked kinematic hardening to model a yield surface whose curvature at the loading point remains constant even as the material strain hardens. He showed that necking strains predicted were highly sensitive to the curvature of the yield surface and that the kinematic hardening results were in better accord with experimental findings than those based on the isotropic hardening yield surface.

In much the same spirit, we address in this paper the sensitivity of flow localization predictions to the curvature of the yield surface of the porous solid. We do this by formulating a family of yield surfaces and associated flow laws in which a given yield surface is incremented with a specific combination of isotropic and kinematic components. Each member of the family is constructed such that under proportional stressing it coincides with Gurson's purely isotropic hardening version. The difference between any two members of the family only shows up when departures from proportional stressing occur. Flow localization calculations similar to those of Yamamoto (1978) and Saje, Pan and Needleman (1982) have been carried out for shear localizations using both the isotropic hardening version of Gurson and the purely kinematic version. The difference between the two sets of predictions is dramatic. It is concluded that the kinematic version, or perhaps a member of the family involving combined isotropic and kinematic hardening, may provide one practical means of circumventing the apparent overly stiff behavior associated with the Gurson model as it now stands.

No attempt will be made in this paper to assess the accuracy of the constitutive models, either by comparison with detailed calculations for void arrays or by direct comparisons with experiments. The limited number of assessments which have been made (e.g., Tvergaard, 1982) suggests that for proportional stressing the Gurson model, or a relatively minor modification of it mentioned later, is at least qualitatively correct. Thus, given the aims of the present study, we feel justified in using the Gurson model as the reference for proportional stressing. Nucleation effects are not considered in this paper since the central issue addressed here does not hinge on nucleation. Such effects may be incorporated in the manner of Saje et al. (1982).

2. Yield functions and rate-constitutive relations

2.1. Yield functions

Gurson's (1977) yield function involves two state parameters, the void volume fraction f and a measure of the current flow stress of the matrix material σ_e. With $\boldsymbol{\Sigma}$ as the macroscopic stress, $\boldsymbol{\Sigma}'$ as its deviator, and $\Sigma_m = \frac{1}{3}\Sigma_{kk}$ as the mean stress, Gurson's condition for yield is

$$\Phi_G(\boldsymbol{\Sigma}, \sigma_e, f) \equiv \frac{3}{2}\frac{\Sigma'_{ij}\Sigma'_{ij}}{\sigma_e^2} + 2f\cosh\left(\frac{3}{2}\frac{\Sigma_m}{\sigma_e}\right) - (1+f^2) = 0. \tag{2.1}$$

Here and throughout the paper Cartesian components of vectors and tensors will be used. Tvergaard (1982) has proposed a modification of this yield function involving different coefficients in the second and third terms. These modifications are readily accommodated in the development which follows, but they will not be considered since they will not effect the *relative* behavior of the various theories.

To introduce a family of combined isotropic/kinematic hardening yield surfaces, let σ_e continue to play the role as a measure of the matrix flow stress, and let σ_y be the *initial yield stress* of the matrix material. The radius of the yield surface of the matrix material is denoted by σ_F and it is taken as

$$\sigma_F = (1-b)\sigma_y + b\sigma_e \tag{2.2}$$

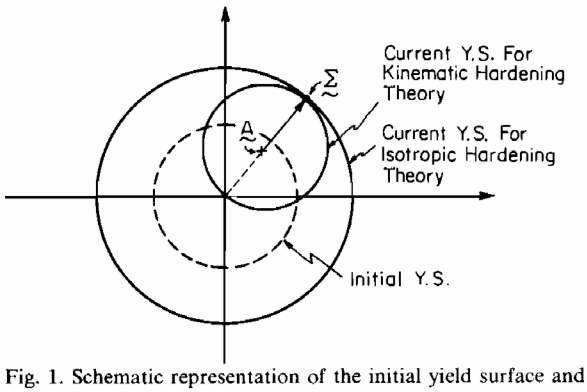

Fig. 1. Schematic representation of the initial yield surface and the current yield surfaces for the isotropic hardening and kinematic hardening theories. The current stress state is $\boldsymbol{\Sigma}$ (the loading point), and the 'center' of the kinematic hardening surface is at $\boldsymbol{A}$.

where the parameter b is assumed to be a constant lying in the range [0,1]. For the family of yield functions given below, the choice $b = 1$ corresponds to isotropic hardening (i.e., Gurson's function (2.1)), while $b = 0$ corresponds to pure kinematic hardening. In the void-free limit ($f = 0$), these two theories reduce to their respective classical limits. The linear relation (2.2) between σ_F and σ_e is the simplest to consider, but the constitutive relation developed below could embrace nearly any dependence of σ_F on σ_e.

Let $\boldsymbol{A}$ be a symmetric tensor which specifies the current 'center' of the yield surface, as depicted in Fig. 1, and let $\boldsymbol{A}'$ denote its deviator. Let

$$\boldsymbol{B} = \boldsymbol{\Sigma} - \boldsymbol{A} \tag{2.3}$$

be the stress difference taken from the center of the yield surface to the loading point, with deviator $\boldsymbol{B}'$ and mean $B_m = \frac{1}{3}B_{kk}$. The yield condition is taken to be

$$\Phi(\boldsymbol{\Sigma}, \boldsymbol{A}, \sigma_F, f) \equiv \frac{3}{2}\frac{B'_{ij}B'_{ij}}{\sigma_F^2} + 2f\cosh\left(\frac{3}{2}\frac{B_m}{\sigma_F}\right) - (1+f^2) = 0. \tag{2.4}$$

2.2. Rate-equations

The form of the rate-equations for the family of relations associated with (2.4) will be stated, and then we will indicate how they become fully determined once the condition is imposed that each member of the family coincides with Gurson's relation for proportional stressing.

For simplicity, it will be assumed that all voids are present prior to stressing and that no new voids are nucleated. The plastic strain-rate in a loading increment is given by

$$D^p_{ij} = \frac{1}{H}\frac{\partial\Phi}{\partial\Sigma_{ij}}\frac{\partial\Phi}{\partial\Sigma_{kl}}\overset{*}{\Sigma}_{kl} \tag{2.5}$$

where

$$\frac{\partial\Phi}{\partial\Sigma_{ij}} = \frac{3B'_{ij}}{\sigma_F^2} + \frac{f}{\sigma_F}\sinh\left(\frac{3}{2}\frac{B_m}{\sigma_F}\right)\delta_{ij} \tag{2.6}$$

and where H is a function of the current state which will be determined later when the relation is brought

into agreement with Gurson's relation. The loading condition requires that the stresses are such that $\Phi = 0$ and that

$$\frac{1}{H}\frac{\partial \Phi}{\partial \Sigma_{kl}}\overset{*}{\Sigma}_{kl} \geqslant 0. \tag{2.7}$$

The choice of stress-rate $\overset{*}{\boldsymbol{\Sigma}}$ will be discussed further below. At this stage we only insist that it be objective and that its principal components coincide with true stress-rates under proportional stressing. By definition, proportional stressing at finite strain requires that the principal stress axes not rotate with respect to the material and that the principal stress components increase in fixed proportion.

The evolution equations for σ_e and f are taken to be the same as those used by Gurson, i.e.,

$$\dot{f} = (1-f)D^{\mathrm{P}}_{kk} \tag{2.8}$$

and

$$\Sigma_{ij}D^{\mathrm{P}}_{ij} = (1-f)\sigma_e\dot{\sigma}_e/h(\sigma_e). \tag{2.9}$$

Here, $h(\sigma_e)$ is the plastic hardening modulus of the matrix material at the current level of σ_e. In terms of true stress–log strain data for the matrix material in uniaxial tension,

$$h = \mathrm{d}\sigma/\mathrm{d}\epsilon^{\mathrm{P}}. \tag{2.10}$$

The evolution equation for the center of the yield surface during a loading increment is taken to be

$$\overset{*}{A}_{ij} = QB_{ij}\frac{\partial \Phi}{\partial \Sigma_{kl}}\overset{*}{\Sigma}_{kl} \tag{2.11}$$

where Q is another function of the current state which will be determined below. With this choice, the change in $\boldsymbol{A}$ is co-directional with $\boldsymbol{B}$ and vanishes continuously for stress increments approaching unloading.

2.3. Coincidence with Gurson's relation for proportional stressing histories

With $b = 1$ so that $\sigma_F = \sigma_e$, equations (2.5) through (2.7), reduce to those of Gurson, i.e., respectively,

$$D^{\mathrm{P}}_{ij} = \frac{1}{H_G}\frac{\partial \Phi_G}{\partial \Sigma_{ij}}\frac{\partial \Phi_G}{\partial \Sigma_{kl}}\overset{*}{\Sigma}_{kl}, \tag{2.12}$$

$$\frac{\partial \Phi_G}{\partial \Sigma_{ij}} = 3\frac{\Sigma'_{ij}}{\sigma_e^2} + \frac{f}{\sigma_e}\sinh\left(\frac{3}{2}\frac{\Sigma_m}{\sigma_e}\right)\delta_{ij} \tag{2.13}$$

and

$$H_G^{-1}\frac{\partial \Phi_G}{\partial \Sigma_{kl}}\overset{*}{\Sigma}_{kl} \geqslant 0. \tag{2.14}$$

These equations, together with (2.8)–(2.10), and the consistency condition for plastic loading, $\dot{\Phi}_G = 0$, lead to Gurson's expression for H_G, i.e.,

$$H_G = \left\{(1-f)^{-1}\frac{h}{\sigma_e^2}\left(\frac{\partial \Phi_G}{\partial \Sigma_{kl}}\Sigma_{kl}\right)^2 - (1-f)\frac{\partial \Phi_G}{\partial f}\frac{\partial \Phi_G}{\partial \Sigma_{kk}}\right\}. \tag{2.15}$$

For proportional stressing, we bring each member ($b \neq 1$) of the family of rate-constitutive relations into coincidence with Gurson's relation by choosing the functions H and Q such that

$$B_{ij}/\sigma_F = \Sigma_{ij}/\sigma_e \tag{2.16}$$

and

$$H^{-1}\frac{\partial \Phi}{\partial \Sigma_{ij}}\frac{\partial \Phi}{\partial \Sigma_{kl}}\overset{*}{\Sigma}_{kl} = H_G^{-1}\frac{\partial \Phi_G}{\partial \Sigma_{ij}}\frac{\partial \Phi_G}{\partial \Sigma_{kl}}\overset{*}{\Sigma}_{kl}. \tag{2.17}$$

Satisfaction of (2.16) ensures that $\Phi = 0$ when $\Phi_G = 0$, while (2.17) ensures the coincidence of plastic strain-rates; σ_e and f will then also evolve exactly as their respective counterparts. The determination of H and Q is facilitated by noting that in proportional stressing $\overset{*}{\boldsymbol{\Sigma}}$, $\overset{*}{\boldsymbol{A}}$, $\boldsymbol{A}$ and $\boldsymbol{B}$ are all co-directional with $\boldsymbol{\Sigma}$. The results of this relatively straightforward, but somewhat lengthy, determination are

$$H = \left\{(1-f)^{-1}\frac{h}{\sigma_F^2}\left(\frac{\partial \Phi}{\partial \Sigma_{ij}}B_{ij}\right)^2 - (1-f)\frac{\sigma_e}{\sigma_F}\frac{\partial \Phi}{\partial f}\frac{\partial \Phi}{\partial \Sigma_{kk}}\right\} \tag{2.18}$$

and

$$Q = (1-b)\left(\frac{\partial \Phi}{\partial \Sigma_{ij}}B_{ij}\right)^{-1}\left\{1 + (1-f)H^{-1}\frac{\sigma_y}{\sigma_F}\frac{\partial \Phi}{\partial f}\frac{\partial \Phi}{\partial \Sigma_{kk}}\right\}. \tag{2.19}$$

We remark in passing that the 'center' of the yield surface, $\boldsymbol{A}$, has a mean component as well as a deviatoric part. Moreover, in the limit $f \to 0$, corresponding to the void-free solid, the mean component of $\boldsymbol{A}$ persists even though it ceases to play any role in the equations. As already stated, the two special cases, $b = 1$ and $b = 0$, reduce to the respective classical theories, J_2 flow theory and J_2 kinematic hardening theory.

2.4. Elastic/plastic equations

As has already been emphasized, the volume fraction of voids is expected to be small, at most several percent, in most applications of the theory, except possibly in the final coalescence stage of failure. Accordingly, following Gurson, we neglect the effect of void volume fraction f on the elastic properties of the material and assume an isotropic relation between the elastic strain-rate and the stress rate according to

$$D_{ij}^e = \frac{1+\nu}{E}\overset{*}{\Sigma}_{ij} - \frac{3\nu}{E}\overset{*}{\Sigma}_m\delta_{ij} \tag{2.20}$$

where E and ν are the Young's modulus and Poisson's ratio of the matrix material.

The total strain-rate, $\boldsymbol{D} = \boldsymbol{D}^e + \boldsymbol{D}^p$, can be expressed as

$$D_{ij} = M_{ijkl}\overset{*}{\Sigma}_{kl} \tag{2.21}$$

where

$$M_{ijkl} = \frac{1+\nu}{2E}\left(\delta_{ik}\delta_{jl} + \delta_{il}\delta_{jk}\right) - \frac{\nu}{E}\delta_{ij}\delta_{kl} + \frac{1}{H}\frac{\partial \Phi}{\partial \Sigma_{ij}}\frac{\partial \Phi}{\partial \Sigma_{kl}} \tag{2.22}$$

assuming loading takes place. The inversion is

$$\overset{*}{\Sigma}_{ij} = L_{ijkl}D_{kl} \tag{2.23}$$

where

$$L_{ijkl} = G\left(\delta_{ik}\delta_{jl} + \delta_{il}\delta_{jk}\right) + \left(K - \tfrac{2}{3}G\right)\delta_{ij}\delta_{kl} - \left(\frac{H\sigma_F^2}{36} + \frac{G}{2\sigma_F^2}B'_{pq}B'_{pq} + K\alpha^2\right)^{-1}\left[\frac{G}{\sigma_F}B'_{ij} + K\alpha\delta_{ij}\right]\left[\frac{G}{\sigma_F}B'_{kl} + K\alpha\delta_{kl}\right] \tag{2.24}$$

and where $G = E/(2(1+\nu))$, $K = E/(3(1-2\nu))$ and

$$\alpha = \tfrac{1}{2}f\,\sinh\left(\tfrac{3}{2}B_m/\sigma_F\right).$$

The loading condition expressed in terms of the strain-rate is

$$\left[\frac{G}{\sigma_F}B'_{ij} + K\alpha\delta_{ij}\right]D_{ij} \geqslant 0. \tag{2.25}$$

In the flow localization studies presented in the next section, the rate of stress $\overset{*}{\boldsymbol{\Sigma}}$ and the rate of shift of the yield surface center $\overset{*}{\boldsymbol{A}}$ will be identified with the Jaumann co-rotational rate. When large rotations of the principal stress axes occur relative to the material, some other choice, such as those discussed by Dienes (1979), Dafalias (1983) or Lee, Mallett and Wertheimer (1983) should be preferred. However, the shear localization phenomena studied in this paper are already fully developed before the occurrence of any significant rotations of the principal stress axes relative to the material, and therefore the Jaumann rate is an acceptable choice. This point is illustrated in the Appendix.

3. Flow localization in plane strain

In this section a study of localization of deformation within a narrow band is carried out to demonstrate the sensitivity of the localization phenomenon to the curvature of the yield surface. Following similar studies by Yamamoto (1978) and Saje et al. (1982), we analyze the problem of an infinite planar band of material with one set of uniform material properties sandwiched within an infinite block of material with different, but uniform, properties. When specialized to plane strain, the geometry of the system is shown in Fig. 2. For appropriately prescribed uniform stressing of the infinite block, the system is characterized by two uniform deformation states, that in the band and that without. If the band material is the weakest, the deformation in the bands develops more rapidly than that in the block until a point is reached where an

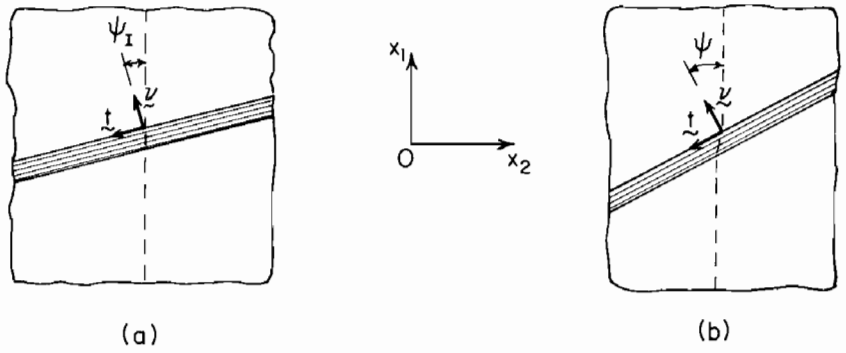

Fig. 2. Band orientation in an infinite block of material in the (a) undeformed state and in the (b) deformed state.

increment of deformation can occur within the band with no corresponding increment outside. This is the onset of localization. Thereafter, additional plastic deformation is confined to the band and elastic unloading occurs without.

3.1. Governing equations

The general framework for the infinite band localization analysis has been given by Rice (1976). We will briefly summarize the governing equations for plane strain, and then present numerical results comparing predictions from the isotropic and kinematic hardening versions of the constitutive law.

Let $\boldsymbol{\nu}$ denote the current unit normal to the band. Denote quantities characterizing the band states by a superscript b and use a similar designation with a superscript o for quantities outside the band. Continuity of velocities across the interfaces between the band and the material without requires that the difference in velocity gradients has the form

$$v^{\mathrm{b}}_{i,j} - v^{\mathrm{o}}_{i,j} = \dot{q}_1 t_i \nu_j + \dot{q}_2 \nu_i \nu_j \tag{3.1}$$

where $\boldsymbol{t}$ is a unit vector parallel to the band in the (x_1, x_2)-plane. Thus, $\dot{q}_1$ measures the rate of development of the shearing difference and $\dot{q}_2$ the relative normal separation-rate.

Let N_{ij} be the Cartesian components of the unsymmetric nominal stress tensor (i.e., the first Piola–Kirchhoff stress). Continuity of traction-rates across the band interfaces requires

$$\left(\dot{N}^{\mathrm{b}}_{ij} - \dot{N}^{\mathrm{o}}_{ij}\right)\nu_i \nu_j = 0 \quad \text{and} \quad \left(\dot{N}^{\mathrm{b}}_{ij} - \dot{N}^{\mathrm{o}}_{ij}\right)\nu_i t_j = 0. \tag{3.2}$$

Using the connection between $\dot{\boldsymbol{N}}$ and the Jaumann stress-rate

$$\dot{N}_{ij} = \overset{*}{\Sigma}_{ij} - \Sigma_{jk} D_{ki} + \Sigma_{ik} W_{jk} + \Sigma_{ij} D_{kk} \tag{3.3}$$

and with $W_{jk} = \frac{1}{2}(v_{j,k} - v_{k,j})$, one can write

$$\dot{N}_{ij} = c_{ijkl} v_{l,k} \tag{3.4}$$

where

$$c_{ijkl} = L_{ijkl} + \tfrac{1}{2}\Sigma_{ik}\delta_{jl} - \tfrac{1}{2}\Sigma_{il}\delta_{kj} - \tfrac{1}{2}\Sigma_{jl}\delta_{ik} - \tfrac{1}{2}\Sigma_{jk}\delta_{il} + \Sigma_{ij}\delta_{kl}. \tag{3.5}$$

The two conditions on the traction-rates (3.2) provide equations for $\dot{q}_1$ and $\dot{q}_2$ as

$$\begin{bmatrix} c^{\mathrm{b}}_{ijkl}\nu_i\nu_j\nu_k t_l & c^{\mathrm{b}}_{ijkl}\nu_i\nu_j\nu_k\nu_l \\ c^{\mathrm{b}}_{ijkl}\nu_i t_j\nu_k t_l & c^{\mathrm{b}}_{ijkl}\nu_i t_j\nu_k\nu_l \end{bmatrix} \begin{Bmatrix} \dot{q}_1 \\ \dot{q}_2 \end{Bmatrix} = \left(c^{\mathrm{o}}_{ijkl} - c^{\mathrm{b}}_{ijkl}\right) v^{\mathrm{o}}_{l,k} \begin{Bmatrix} \nu_i\nu_j \\ \nu_i t_j \end{Bmatrix}. \tag{3.6}$$

Given an initial set of material properties and given a history of $v^{\mathrm{o}}_{i,j}$, one can use (3.6), together with the equations governing the evolution of the two sets of constitutive moduli and associated quantities, and the evolution of $\boldsymbol{\nu}$ and $\boldsymbol{t}$, to solve for the two evolving deformation states. If (3.6) is written in matrix form as $A\dot{q} = b$, then it is clear that the onset of localization occurs when $\det(A) = 0$. Either the velocity gradients or some combination of stress-rates and velocity gradients consistent with plane strain may be imposed on the block of material outside the band prior to localization. Because the deformation-rates within the band become large compared to those outside the band as the onset of localization is approached, it is usually convenient for numerical purposes to let some monotonically increasing quantity in the band such as $\dot{q}_1$, or some component of the velocity gradient, serve as the independent variable in the integration process. This same quantity can be used to continue the deformation through the point where $\det(A) = 0$.

3.2. Numerical results

Two sets of computations have been carried out, for plane strain tension and for a simulation of necking in plane strain tension. In each case, the material in the semi-infinite block outside the band is taken to be void-free ($f_I^o = 0$), and the initial void volume fraction within the band is taken as either $f_I^b = 0.001$ or $f_I^b = 0.01$. In all cases both inside and outside the band, the matrix material was prescribed by the uniaxial stress–strain relation

$$\epsilon/\epsilon_y = \begin{cases} \sigma/\sigma_y, & \sigma \leqslant \sigma_y, \\ (\sigma/\sigma_y)^n, & \sigma > \sigma_y \end{cases} \tag{3.7}$$

where $\epsilon_y = \sigma_y/E$ is the initial elastic yield strain, which was taken to be 0.0033. Results will be reported for two n-values, 5 and 10.

In plane strain tension, the semi-infinite block is subject to

$$D_{11}^o = v_{1,1}^o > 0, \qquad v_{1,2}^o = v_{2,1}^o = 0, \qquad \Sigma_{22}^0 = 0 \tag{3.8}$$

prior to localization. Let ϵ_c^o denote the logarithmic strain in the material outside the band in the 1-direction when the localization condition is met. This localization strain has been computed over a range of initial band orientations ψ_I. The results are shown in Fig. 3. In these plots, the solid line curves give ϵ_c^o as a function of the initial band orientation ψ_I, while the dashed line curves give ϵ_c^o as a function of the orientation of the band at localization ψ_c. In each plot, the upper set of curves corresponds to the isotropic hardening version of the constitutive model (i.e., $b = 1$, Gurson's version) and the lower set corresponds to the kinematic hardening version with $b = 0$.

The difference between the predictions for the two versions of the constitutive model are fairly significant, particularly if the localization strains are converted to stretches. In each example, the minimum localization strain occurs at a band orientation in the range $40° < \psi_c < 50°$. For a given level of f_I^b, the range of initial band orientation ψ_I over which the material is susceptible to localization is considerably larger for the kinematic hardening solid because the localization strains are so much lower resulting in less rotation from ψ_I to ψ_c. Perhaps the most dramatic difference is the level of initial void volume fraction f_I^b needed to bring about a given minimum localization strain. From Fig. 3 and Table 1 it is seen that the minimum localization strain for the kinematic hardening solid with $f_I^b = 0.001$ is only slightly larger than the minimum localization strain for the isotropic hardening solid with $f_I^b = 0.01$.

For the case with $n = 5$ and $f_I^b = 0.001$, curves of the void volume fraction in the band at localization, f_c^b, are plotted as a function of ψ_c in Fig. 4, and the values associated with the minimum localization strain are included in Table 1. (The dashed curves in Fig. 4 apply to the necking simulation which will be

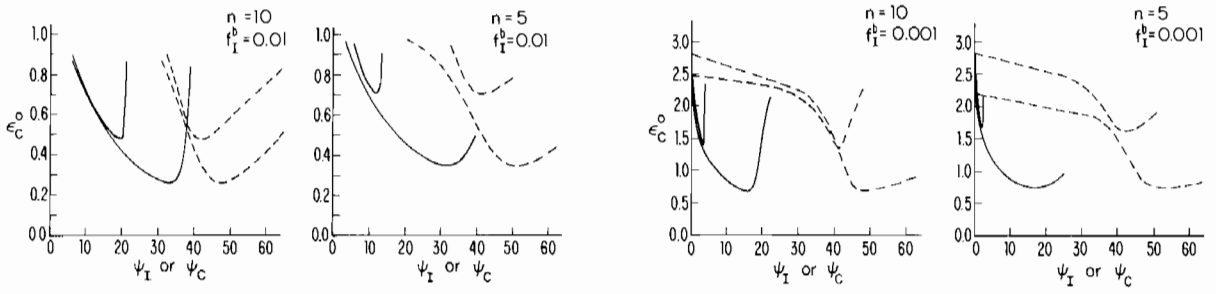

Fig. 3. True strain in the block in the x_1-direction at localization, ϵ_c^o, as a function of the angle at which the band is oriented, ψ (_____ 148: initial angle ψ_I; – – –: angle at localization ψ_c). Plane strain tension.

Table 1
The minimum value of ϵ_c^o, $(\epsilon_c^o)_{min}$, and the corresponding value of f_c^b.

Isotropic hardening without necking				Kinematic hardening without necking			
n	f_I^b	$(\epsilon_c^o)_{min}$	f_c^b	n	f_I^b	$(\epsilon_c^o)_{min}$	f_c^b
5	0.001	1.627	0.027	5	0.001	0.735	0.004
10	0.001	1.327	0.011	10	0.001	0.684	0.003
5	0.01	0.707	0.058	5	0.01	0.352	0.021
10	0.01	0.476	0.036	10	0.01	0.261	0.018
Isotropic hardening with necking				Kinematic hardening with necking			
n	f_I^b	$(\epsilon_c^o)_{min}$	f_c^b	n	f_I^b	$(\epsilon_c^o)_{min}$	f_c^b
5	0.001	1.024	0.023	5	0.001	0.596	0.005
10	0.001	0.828	0.011	10	0.001	0.542	0.004
5	0.01	0.553	0.048	5	0.01	0.331	0.021
10	0.01	0.376	0.034	10	0.01	0.243	0.019

discussed below.) Here, too, the difference between the predictions of the two versions of the constitutive model are striking. For the kinematic hardening solid the ratio of f_c^b to f_I^b is between 2 and 4, while the corresponding ratio for the isotropic hardening solid is between 4 and 20. Particularly for the kinematic hardening solid, it is evident that localization can set in at very low void volume fractions as discussed in the Introduction.

To simulate the triaxial stress state that develops at the center of a neck in a plane strain tension specimen, we follow Saje, Pan and Needleman (1982) and use the Bridgman expression for the transverse component of stress in the neck,

$$\Sigma_{22}^o = \left[\frac{\ln(1+\frac{1}{2}r)}{1+\ln(1+\frac{1}{2}r)}\right]\Sigma_{11}^o \tag{3.9}$$

where r is the ratio of the thickness through the minimum section of the neck to its radius of curvature.

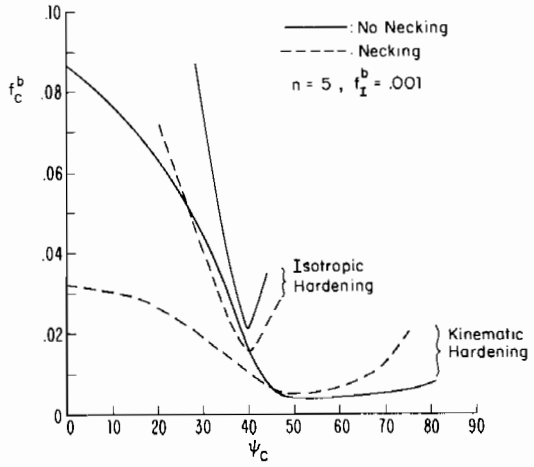

Fig. 4. Void volume fraction in band at localization as a function of orientation of band at localization. Initial void volume fraction of 0.001 in all cases.

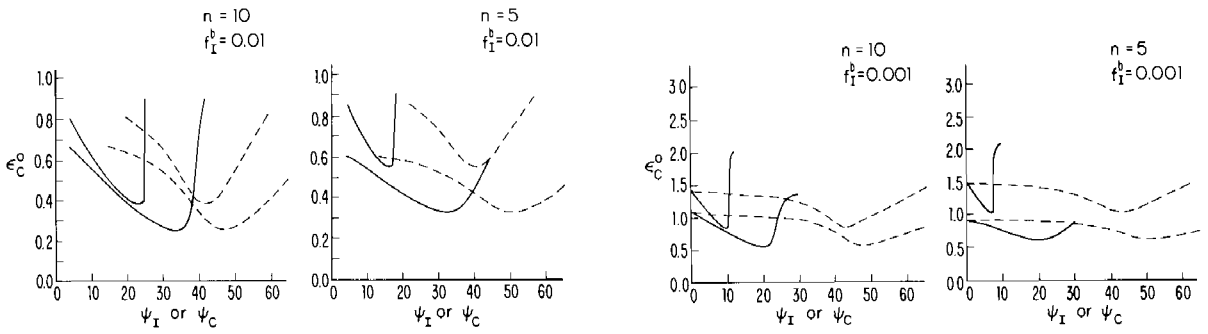

Fig. 5. True strain in the block in the x_1-direction at localization, ϵ_c^o, as a function of the angle at which the band is oriented, ψ (_____: initial angle ψ_1, – – –:angle at localization ψ_c). Simulation of necking in plane strain.

This ratio is zero for $\epsilon_1 \leqslant 1/n$ and is taken to be

$$r = 0.833(\epsilon_1 - 1/n) \tag{3.10}$$

for $\epsilon_1 > 1/n$, although this latter expression was only established experimentally for round specimens. Thus, in the localization study the material outside the band is subject to a plane strain history with

$$D_{11}^o > 0, \qquad v_{1,2}^o = v_{2,1}^o = 0 \quad \text{with } \dot{\Sigma}_{22}^o = \rho \dot{\Sigma}_{11}^o \tag{3.11}$$

where ρ is derived from (3.9) using the constitutive relation for the material outside the band.

The results for the necking simulation are shown in Fig. 5 and are presented in the same manner as for the plane strain tension case. The discrepancy between the predictions of the two versions of the theory is somewhat less pronounced because the larger strains sustained by the isotropic hardening material leads to higher triaxiality and thus accelerated void growth. The void volume fractions at localization are included in Fig. 4. The large differences noted in connection with the plane strain tension case are evident in the necking simulation as well.

4. Conclusions

Flow localization predictions have been shown to be highly sensitive to the curvature of the yield surface. Specifically, the localization strains from isotropic hardening and kinematic hardening versions of otherwise identical constitutive laws differ significantly. Even more sensitive is the initial void volume fraction associated with a given localization strain. In some examples, the initial void volume fraction for the isotropic hardening version was almost ten times that for the kinematic version for comparable localization strains.

The sensitivity of the predictions to yield surface curvature is not surprising considering the well known difficulties of applying isotropic hardening theory to plastic instability problems. In an earlier study, Hutchinson and Tvergaard (1981) found that shear localization in plane strain is essentially impossible in a J_2 isotropic hardening material with no voids present, while shear localization can occur in the corresponding kinematic hardening material. Nevertheless, the issue of invoking isotropic hardening does not seem to have received enough consideration for dilatant plasticity models. To some extent, this lack of consideration may be because the dilatational aspects of the theory helps ameliorate the overly stiff response of the classical isotropic hardening theory. Whether the dilatational response is sufficient in this regard is not yet clear. The void volume fractions of interest for high quality materials are very small, as has been emphasized. It seems to us unlikely that inclusion of the dilatational response alone, without modification of the isotropic hardening assumption, will be sufficient to realistically model actual material behavior.

Acknowledgement

The work of M.E. Mear was supported in part by a grant from ALCOA and by the Division of Applied Sciences, Harvard University. The work of J.W. Hutchinson was supported in part by the National Science Foundation under Grant MEA-82-13925 and by the Division of Applied Sciences, Harvard University. Stimulating discussions with O. Richmond are acknowledged.

Appendix. An alternative choice of stress-rate

The Jaumann co-rotational rate was used in carrying out the localization calculations presented in Section 3. It has been shown that the use of this rate leads to erroneous results when kinematic hardening theory is used to model a material block being subjected to extensive shearing deformation. A rate which is objective and which gives plausible results for this deformation history and material model is based on $\boldsymbol{\Omega} = \dot{\boldsymbol{R}} \cdot \boldsymbol{R}^{\mathrm{t}}$ rather than $\boldsymbol{W}$ (Dafalias, 1983; and Dienes, 1979). Here, $\boldsymbol{R}$ is the orthogonal rotation tensor (see below) and $\boldsymbol{W}$ is the spin tensor. The relation of this rate to the material rate of Cauchy stress takes the same form as the Jaumann rate, namely

$$\overset{*}{\dot{\Sigma}}_{ij} = \dot{\Sigma}_{ij} - \Omega_{ik}\Sigma_{kj} + \Sigma_{ik}\Omega_{kj}. \tag{A.1}$$

To explore the appropriateness of the Jaumann rate for the calculations carried out in Section 3, the first case shown in Fig. 3 is reexamined using the alternative rate described above. The usefulness of this rate in incremental plasticity is not addressed here; only the effect of using it rather than the Jaumann rate is explored. It is found that the predictions of localization strains obtained by using the Jaumann rate and the alternative are not very different, and it is concluded that it is adequate to use the Jaumann rate in affecting the localization calculations presented here.

Relation of $\boldsymbol{\Omega}$ to $\boldsymbol{W}$

The development given below follows that of Dienes (1979), although different notation is used in some places. A more general, but related, treatment is given by Nemat-Nasser (1983). As before, the components of all tensors are referred to a single stationary Cartesian coordinate system, oriented as shown in Fig. 2.

The deformation gradient, $\boldsymbol{F}$, can be decomposed as

$$\boldsymbol{F} = \boldsymbol{V} \cdot \boldsymbol{R} \tag{A.2}$$

where $\boldsymbol{V}$ is the left stretch tensor and $\boldsymbol{R}$ is the orthogonal rotation tensor. The spatial velocity gradient, $\boldsymbol{L}$, can be split into its symmetric and antisymmetric parts, which are the rate of deformation tensor $\boldsymbol{D}$ and the spin tensor $\boldsymbol{W}$, respectively. It can be related to $\boldsymbol{F}$ by

$$\boldsymbol{L} = \dot{\boldsymbol{F}} \cdot \boldsymbol{F}^{-1} \tag{A.3}$$

and can be expressed in terms of $\boldsymbol{V}$ and $\boldsymbol{R}$ by use of (A.2) as

$$\boldsymbol{L} = \dot{\boldsymbol{V}} \cdot \boldsymbol{V}^{-1} + \boldsymbol{V} \cdot \boldsymbol{\Omega} \cdot \boldsymbol{V}^{-1} \tag{A.4}$$

where $\boldsymbol{\Omega} = \dot{\boldsymbol{R}} \cdot \boldsymbol{R}^{\mathrm{t}}$.

Post multiplying this last equation by $\boldsymbol{V}$ gives

$$\dot{\boldsymbol{V}} = \boldsymbol{L} \cdot \boldsymbol{V} - \boldsymbol{V} \cdot \boldsymbol{\Omega} \tag{A.5}$$

and forming $\dot{\boldsymbol{V}} - \dot{\boldsymbol{V}}^{\mathrm{t}}$ ($= \boldsymbol{0}$ since $\boldsymbol{V}$ is symmetric) gives

$$\boldsymbol{Z} = \boldsymbol{V} \cdot \boldsymbol{H} + \boldsymbol{H} \cdot \boldsymbol{V} \tag{A.6}$$

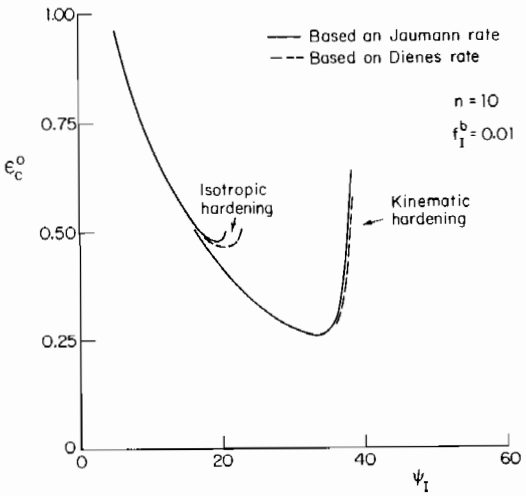

Fig. 6. Comparison of results based on two choices of stress-rates used in formulating the constitutive model. True strain in block at localization, ϵ_c^o, as a function of initial orientation of the band, ψ_I. Plane strain tension with $n = 10$, $\epsilon_y = 0.0033$, $f_I^o = 0$ and $f_I^b = 0.01$.

where $\boldsymbol{Z} = \boldsymbol{D} \cdot \boldsymbol{V} - \boldsymbol{V} \cdot \boldsymbol{D}$ is skew symmetric as is $\boldsymbol{H} = \boldsymbol{\Omega} - \boldsymbol{W}$. In the present case $\boldsymbol{H}^o = \boldsymbol{0}$ and the only nonzero components of $\boldsymbol{H}^b$ are $H_{12}^b = -H_{21}^b$ where, from (A.6),

$$H_{12}^b = \frac{V_{12}^b}{V_{11}^b + V_{22}^b}\left(D_{11}^b - D_{22}^b\right) + \frac{\left(V_{22}^b - V_{11}^b\right)}{V_{11}^b + V_{22}^b} D_{12}^b. \tag{A.7}$$

Numerical results and discussion

The case of $f_I^b = 0.01$, $f_I^o = 0.0$, $n = 10$, and $\epsilon_y = 0.0033$ is examined. The results of the calculations for the true strain in the x_1-direction at localization, ϵ_c^o, as a function of the initial band orientation, ψ_1, are shown in Fig. 6 for both the isotropic hardening theory and the kinematic hardening theory. The solid lines are the results of the calculation when the Jaumann rate is employed, and the dashed lines are the results when the objective rate is based on $\boldsymbol{\Omega}$ rather than $\boldsymbol{W}$. Note that the only nonzero components of $\boldsymbol{\Omega}^b$ are $\Omega_{12}^b = -\Omega_{21}^b = W_{12}^b + H_{12}^b$ where $W_{12}^b = -\frac{1}{2}\dot{q}_1$, and that the components of the stretch tensor are updated at each step of the deformation via (A.5).

The results for the two rates are essentially identical for the kinematic hardening theory, and they are close for the isotropic hardening theory except for a spreading of the ϵ_c^o vs. ψ_1 curve around $\psi_I = 20°$. Considering the assumptions involved in the infinite band calculations and the information which they provide, we conclude that the Jaumann rate is an adequate objective rate to use in performing them.

References

Dafalias, Y.F. (1983), "Corotational rates for kinematic hardening at large plastic deformations", *J. Appl. Mech. 50*, 561.

Dienes, J.K. (1979), "On the analysis of rotation and stress rate in deforming bodies", *Acta Mechanica 32*, 217.

Gurson, A.L. (1977), "Continuum theory of ductile rupture by void nucleation and growth – Part I. Yield criteria and flow rules for porous ductile media", *J. Engrg. Mater. Technol. 99*, 2.

Hutchinson, J.W. and V. Tvergaard (1981), "Shear band formation in plane strain", *Internat. J. Solids Structures 17*, 451.

Lee, E.H., R.L. Mallett and T.B. Wertheimer (1983), "Stress analysis for kinematic hardening in finite-deformation plasticity", *J. Appl. Mech. 50*, 554.

Nemat-Nasser, S. (1983), "On finite plastic flow of crystalline solids and geomaterials", *J. Appl. Mech. 50*, 1114.

Rice, J.R. (1976), "The localization of plastic deformation", in: W.T. Koiter, ed., *Theoretical and Applied Mechanics*, North-Holland, Amsterdam, 207.

Saje, M., J. Pan and A. Needleman (1982), "Void nucleation effects on shear localization in porous plastic solids", *Internat. J. Fracture 19*, 163.

Tvergaard, V. (1978), "Effect of kinematic hardening on localized necking in biaxially stretched sheets", *Internat. J. Mech. Sci. 20*, 651.

Tvergaard, V. (1982), "On localization in ductile materials containing spherical voids", *Internat. J. Fracture 18*, 237.

Yamamoto, H. (1978), "Conditions for shear localization in the ductile fracture of void-containing materials", *Internat. J. Fracture 14*, 347.